KEK preprint 2001-150
Belle preprint 2001-20

Measurement of $\mathcal{B}(\bar{B}^0 \to D^+\ell^-\bar{\nu})$ and Determination of $|V_{cb}|$

Belle Collaboration

K. Abe[9], K. Abe[43], R. Abe[32], T. Abe[44], I. Adachi[9], Byoung Sup Ahn[17], H. Aihara[45], M. Akatsu[25], Y. Asano[50], T. Aso[49], V. Aulchenko[2], T. Aushev[14], A. M. Bakich[41], Y. Ban[36], E. Banas[30], S. Behari[9], P. K. Behera[51], A. Bondar[2], A. Bozek[30], T. E. Browder[8], B. C. K. Casey[8], P. Chang[29], Y. Chao[29], B. G. Cheon[40], R. Chistov[14], S.-K. Choi[7], Y. Choi[40], L. Y. Dong[12], A. Drutskoy[14], S. Eidelman[2], V. Eiges[14], C. W. Everton[23], F. Fang[8], H. Fujii[9], C. Fukunaga[47], M. Fukushima[11], N. Gabyshev[9], A. Garmash[2,9], T. Gershon[9], A. Gordon[23], R. Guo[27], J. Haba[9], H. Hamasaki[9], K. Hanagaki[37], F. Handa[44], K. Hara[34], T. Hara[34], N. C. Hastings[23], H. Hayashii[26], M. Hazumi[9], E. M. Heenan[23], I. Higuchi[44], T. Higuchi[45], T. Hojo[34], T. Hokuue[25], Y. Hoshi[43], K. Hoshina[48], S. R. Hou[29], W.-S. Hou[29], S.-C. Hsu[29], H.-C. Huang[29], Y. Igarashi[9], T. Iijima[9], H. Ikeda[9], A. Ishikawa[25], H. Ishino[46], R. Itoh[9], H. Iwasaki[9], Y. Iwasaki[9], D. J. Jackson[34], P. Jalocha[30], H. K. Jang[39], J. H. Kang[54], J. S. Kang[17], P. Kapusta[30], N. Katayama[9], H. Kawai[3], H. Kawai[45], N. Kawamura[1], T. Kawasaki[32], H. Kichimi[9], D. W. Kim[40], Heejong Kim[54], H. J. Kim[54], H. O. Kim[40], Hyunwoo Kim[17], S. K. Kim[39], T. H. Kim[54], K. Kinoshita[5], H. Konishi[48], S. Korpar[22,15], P. Križan[21,15], P. Krokovny[2], R. Kulasiri[5], S. Kumar[35], A. Kuzmin[2], Y.-J. Kwon[54], J. S. Lange[6], G. Leder[13], S. H. Lee[39], D. Liventsev[14], R.-S. Lu[29], J. MacNaughton[13], T. Matsubara[45], S. Matsumoto[4], T. Matsumoto[25], Y. Mikami[44], K. Miyabayashi[26], H. Miyake[34], H. Miyata[32], G. R. Moloney[23], S. Mori[50], T. Mori[4], A. Murakami[38], T. Nagamine[44], Y. Nagasaka[10], Y. Nagashima[34],

T. Nakadaira[45], E. Nakano[33], M. Nakao[9], J. W. Nam[40], Z. Natkaniec[30], K. Neichi[43], S. Nishida[18], O. Nitoh[48], S. Noguchi[26], T. Nozaki[9], S. Ogawa[42], T. Ohshima[25], T. Okabe[25], S. Okuno[16], S. L. Olsen[8], W. Ostrowicz[30], H. Ozaki[9], P. Pakhlov[14], H. Palka[30], C. S. Park[39], C. W. Park[17], H. Park[19], K. S. Park[40], L. S. Peak[41], J.-P. Perroud[20], M. Peters[8], L. E. Piilonen[52], J. L. Rodriguez[8], N. Root[2], M. Rozanska[30], K. Rybicki[30], J. Ryuko[34], H. Sagawa[9], Y. Sakai[9], H. Sakamoto[18], M. Satapathy[51], A. Satpathy[9,5], S. Schrenk[5], S. Semenov[14], K. Senyo[25], M. E. Sevior[23], H. Shibuya[42], B. Shwartz[2], J. B. Singh[35], S. Stanič[50], A. Sugiyama[25], K. Sumisawa[9], T. Sumiyoshi[9], S. Suzuki[53], S. Y. Suzuki[9], S. K. Swain[8], T. Takahashi[33], F. Takasaki[9], M. Takita[34], K. Tamai[9], N. Tamura[32], J. Tanaka[45], M. Tanaka[9], Y. Tanaka[24], G. N. Taylor[23], Y. Teramoto[33], M. Tomoto[9], T. Tomura[45], S. N. Tovey[23], K. Trabelsi[8], T. Tsuboyama[9], T. Tsukamoto[9], S. Uehara[9], K. Ueno[29], Y. Unno[3], S. Uno[9], Y. Ushiroda[9], K. E. Varvell[41], C. C. Wang[29], C. H. Wang[28], J. G. Wang[52], M.-Z. Wang[29], Y. Watanabe[46], E. Won[39], B. D. Yabsley[9], Y. Yamada[9], M. Yamaga[44], A. Yamaguchi[44], H. Yamamoto[44], Y. Yamashita[31], S. Yanaka[46], J. Yashima[9], M. Yokoyama[45], K. Yoshida[25], Y. Yuan[12], Y. Yusa[44], C. C. Zhang[12], J. Zhang[50], H. W. Zhao[9], Y. Zheng[8], V. Zhilich[2], and D. Žontar[50]

[1] *Aomori University, Aomori*
[2] *Budker Institute of Nuclear Physics, Novosibirsk*
[3] *Chiba University, Chiba*
[4] *Chuo University, Tokyo*
[5] *University of Cincinnati, Cincinnati OH*
[6] *University of Frankfurt, Frankfurt*
[7] *Gyeongsang National University, Chinju*
[8] *University of Hawaii, Honolulu HI*
[9] *High Energy Accelerator Research Organization (KEK), Tsukuba*
[10] *Hiroshima Institute of Technology, Hiroshima*
[11] *Institute for Cosmic Ray Research, University of Tokyo, Tokyo*
[12] *Institute of High Energy Physics, Chinese Academy of Sciences, Beijing*
[13] *Institute of High Energy Physics, Vienna*
[14] *Institute for Theoretical and Experimental Physics, Moscow*
[15] *J. Stefan Institute, Ljubljana*
[16] *Kanagawa University, Yokohama*
[17] *Korea University, Seoul*
[18] *Kyoto University, Kyoto*
[19] *Kyungpook National University, Taegu*
[20] *IPHE, University of Lausanne, Lausanne*
[21] *University of Ljubljana, Ljubljana*

[22] University of Maribor, Maribor
[23] University of Melbourne, Victoria
[24] Nagasaki Institute of Applied Science, Nagasaki
[25] Nagoya University, Nagoya
[26] Nara Women's University, Nara
[27] National Kaohsiung Normal University, Kaohsiung
[28] National Lien-Ho Institute of Technology, Miao Li
[29] National Taiwan University, Taipei
[30] H. Niewodniczanski Institute of Nuclear Physics, Krakow
[31] Nihon Dental College, Niigata
[32] Niigata University, Niigata
[33] Osaka City University, Osaka
[34] Osaka University, Osaka
[35] Panjab University, Chandigarh
[36] Peking University, Beijing
[37] Princeton University, Princeton NJ
[38] Saga University, Saga
[39] Seoul National University, Seoul
[40] Sungkyunkwan University, Suwon
[41] University of Sydney, Sydney NSW
[42] Toho University, Funabashi
[43] Tohoku Gakuin University, Tagajo
[44] Tohoku University, Sendai
[45] University of Tokyo, Tokyo
[46] Tokyo Institute of Technology, Tokyo
[47] Tokyo Metropolitan University, Tokyo
[48] Tokyo University of Agriculture and Technology, Tokyo
[49] Toyama National College of Maritime Technology, Toyama
[50] University of Tsukuba, Tsukuba
[51] Utkal University, Bhubaneswer
[52] Virginia Polytechnic Institute and State University, Blacksburg VA
[53] Yokkaichi University, Yokkaichi
[54] Yonsei University, Seoul

Abstract

We present a measurement of the branching fraction for the semileptonic B decay $\bar{B}^0 \to D^+\ell^-\bar{\nu}$, where ℓ^- can be either an electron or a muon. We find $\Gamma(\bar{B}^0 \to D^+\ell^-\bar{\nu}) = (13.79 \pm 0.76 \pm 2.51)$ ns^{-1}, and the resulting branching fraction $\mathcal{B}(\bar{B}^0 \to D^+\ell^-\bar{\nu}) = (2.13 \pm 0.12 \pm 0.39)\%$, where the first error is statistical and the second systematic. We also investigate the $\bar{B}^0 \to D^+\ell^-\bar{\nu}$ form factor and the implications of the result for $|V_{cb}|$. From a fit to the differential decay distribution we obtain the rate normalization $|V_{cb}|F_D(1) = (4.11 \pm 0.44 \pm 0.52) \times 10^{-2}$. Using a theoretical calculation of $F_D(1)$, the Cabibbo-Kobayashi-Maskawa matrix element $|V_{cb}| = (4.19 \pm 0.45 \pm$

$0.53 \pm 0.30) \times 10^{-2}$ is obtained, where the last error comes from the theoretical uncertainty of $F_D(1)$. The results are based on a data sample of 10.2 fb^{-1} recorded at the $\Upsilon(4S)$ resonance with the Belle detector at the KEKB e^+e^- collider.

Key words: CKM matrix, Semileptonic, B decay
PACS: 12.15.Hh, 13.30.Ce, 13.20.Hw

1 Introduction

In the Standard Model of electroweak interactions, the elements of the Cabibbo-Kobayashi-Maskawa (CKM) quark mixing matrix [1] are constrained by unitarity. Therefore, experimental measurements of the precise values of the CKM matrix elements are important to understand the phenomenology of weak interactions.

In the framework of Heavy Quark Effective Theory (HQET) [2], the semileptonic decay $\bar{B}^0 \to D^+\ell^-\bar{\nu}$ is amongst the cleanest modes that can be used to measure the CKM matrix element $|V_{cb}|$. The differential decay rate for $\bar{B}^0 \to D^+\ell^-\bar{\nu}$ can be expressed as [3]

$$\frac{d\Gamma}{dy} = \frac{G_F^2|V_{cb}|^2}{48\pi^3}(m_{\bar{B}^0} + m_{D^+})^2 m_{D^+}^3 (y^2-1)^{3/2} F_D^2(y), \tag{1}$$

where G_F is the Fermi coupling constant, and $m_{\bar{B}^0}$ and m_{D^+} are the masses of the $\bar{B}^0$ and D^+ mesons respectively. The variable y denotes the inner product of the $\bar{B}^0$ and D^+ meson four-velocities, which is related to q^2, the mass squared of the lepton-neutrino system:

$$y = v_{\bar{B}^0} \cdot v_{D^+} = \frac{m_{\bar{B}^0}^2 + m_{D^+}^2 - q^2}{2m_{\bar{B}^0}m_{D^+}},\ q^2 = (p_{l^-} + p_{\bar{\nu}})^2, \tag{2}$$

and $F_D(y)$ is the form factor. By extrapolating the measured $|V_{cb}|F_D(y)$ to the point of zero recoil of the D^+ meson, $|V_{cb}|$ can be determined using a theoretical prediction of $F_D(1)$. In this paper p represents the four-momentum vector of the particle in subscript, while $\vec{p}$ denotes the three-momentum vector in the center of mass (CM) frame and $\vec{p}_{lab}$ is the three-momentum vector in the laboratory frame.

$|V_{cb}|$ measurements made using $\bar{B} \to D\ell^-\bar{\nu}$ decays are less precise than those made using $\bar{B} \to D^*\ell^-\bar{\nu}$, due to the suppressed decay rate near the point of zero recoil, substantial feed down from $\bar{B} \to D^*\ell^-\bar{\nu}$ and the large combinatoric background from fake D mesons. Nevertheless, the $\bar{B} \to D\ell^-\bar{\nu}$ measurement provides a consistency check, and allows a test of heavy-quark symmetry [4] through the precise measurement of the form factor. Furthermore, this decay has one experimental advantage over $\bar{B} \to D^*\ell^-\bar{\nu}$ as there is no slow pion involved.

The $\bar{B}^0 \to D^+\ell^-\bar{\nu}$ decay is preferred to $B^- \to D^0\ell^-\bar{\nu}$ because it has much less feed-down background from excited charm meson states. Good particle identification and vertexing capabilities allow effective reduction of the combinatoric background.

In this paper we report measurements of the branching fraction of the semileptonic decay $\bar{B}^0 \to D^+\ell^-\bar{\nu}$, the CKM matrix element $|V_{cb}|$ and the form factor $F_D(y)$. The lepton ℓ can be either an electron or a muon, and the use of the charge-conjugate mode is implied.

The data sample used in this analysis was collected with the Belle detector [5] at KEKB [6], an asymmetric e^+e^- collider. The data sample has an integrated luminosity of 10.2 fb^{-1} and contains 10.8×10^6 $B\bar{B}$ pairs. Another data sample with an integrated luminosity of 0.6 fb^{-1} was taken at an energy 60 MeV below the $\Upsilon(4S)$ resonance, and is used as a control sample to check the $e^+e^- \to q\bar{q}$ continuum background determination.

2 Belle detector

Belle is a large solid-angle spectrometer based on a 1.5 T superconducting solenoid magnet. Charged particle tracking is provided by a silicon vertex detector (SVD) and a central drift chamber (CDC) that surround the interaction region. The SVD consists of three approximately cylindrical layers of double-sided silicon strip detectors; one side of each detector measures the z coordinate and the other the $r-\phi$ coordinate. The CDC has 50 cylindrical layers of anode wires; the inner three layers have instrumented cathodes for z coordinate measurements. Eighteen of the wire layers are inclined at small angles to provide small-angle stereo measurements of z coordinates along the particle trajectories. The charged particle acceptance covers the laboratory polar angle between $\theta = 17^\circ$ and 150°, corresponding to about 92% of the full CM frame solid angle. The momentum resolution for charged tracks is determined from cosmic rays and $e^+e^- \to \mu^+\mu^-$ events to be $(\sigma_{|\vec{p}_t|}/|\vec{p}_t|)^2 = (0.0019|\vec{p}_t|)^2 + (0.0030)^2$, where $\vec{p}_t$ is the transverse momentum in GeV/c.

Charged hadron identification is provided by dE/dx measurements in the CDC, a mosaic of 1188 aerogel Čerenkov counters (ACC), and a barrel-like array of 128 time-of-flight scintillation counters (TOF). The dE/dx measurements have a resolution for hadron tracks of 6.9% and are useful for π/K separation for $|\vec{p}_{lab}| < 0.8$ GeV/c and $|\vec{p}_{lab}| > 2.5$ GeV/c. The TOF system has a time resolution for hadrons of $\sigma \simeq 100$ ps and provides π/K separation for $|\vec{p}_{lab}| < 1.2$ GeV/c. The ACC covers the range 1.2 GeV/$c < |\vec{p}_{lab}| < 3.5$ GeV/c, and the refractive indices of the ACC elements vary with polar angle to match the kinematics of the asymmetric energy collisions. High momentum tagged kaons and pions from kinematically selected $D^{*+} \to D^0\pi^+$, $D^0 \to K^-\pi^+$ decays are used to determine a charged kaon identification efficiency of 88% and a misidentification probability of 9%.

Electromagnetic showering particles are detected in an array of 8736 CsI(Tl)

crystals located in the magnetic volume covering the same solid angle as the charged particle tracking system. The energy resolution for electromagnetic showers is $(\sigma_E/E)^2 = (0.013)^2 + (0.0007/E)^2 + (0.008/E^{1/4})^2$, where E is in GeV. Neutral pions are detected via their $\pi^0 \to \gamma\gamma$ decay. The π^0 mass resolution varies slowly with energy, averaging $\sigma = 4.9$ MeV/c^2. For a $\pm 3\sigma$ mass selection requirement, the overall detection efficiency for neutral pions from $B\bar{B}$ events (including the effects of geometrical acceptance) is $\sim 40\%$.

Electron identification in Belle is based on a combination of dE/dx measurements in the CDC, the response of the ACC, the position and shape of the electromagnetic shower, and the ratio $E/|\vec{p}_{lab}|$ of cluster energy registered in the calorimeter and particle momentum. The electron identification efficiency, determined by embedding Monte Carlo (MC) [7] tracks in multihadron data, is greater than 92% for tracks with $|\vec{p}_{lab}| > 1.0$ GeV/c. The hadron misidentification probability, determined from $K^0_S \to \pi^+\pi^-$ decays, is below 0.3%.

The 1.5 T magnetic field is returned via an iron yoke that is instrumented to detect muons and K^0_L mesons. This detection system consists of alternating layers of charged-particle detectors and 4.7 cm thick steel plates. The total steel thickness of 65.8 cm plus the material of the inner detector corresponds to 4.7 nuclear interaction lengths at normal incidence. The system covers polar angles between $\theta = 20^\circ$ and 155°; the overall muon identification efficiency, determined by a track embedding study similar to that used for the electron case, is greater than 87% for tracks with $|\vec{p}_{lab}| > 1$ GeV/c. The corresponding pion misidentification probability determined from inclusive $K^0_S \to \pi^+\pi^-$ decays is less than 2%.

3 Event selection and analysis procedure

3.1 Event selection

For hadronic event selection, we require that each event have at least 5 well-reconstructed charged tracks, a total visible energy of at least 0.15 times the CM energy and an event vertex that is consistent with the known interaction point. Continuum background events are suppressed by requiring the normalized second Fox-Wolfram moment [8] to be less than 0.4.

This analysis is based on the neutrino reconstruction method, which exploits the hermeticity of the detector and the near zero value of the neutrino mass. This method was originally developed by the CLEO collaboration for the measurement of $B \to \pi\ell\nu$ and $\rho(\omega)\ell\nu$ decays [9].

We extract information on the neutrino from the missing momentum ($\vec{p}_{\rm miss}$) and missing energy ($E_{\rm miss}$) in each event. In the CM frame, the total momentum of the system is zero, and the total energy is the sum of the two beam energies ($E_{\rm beam}$). The missing energy, momentum and missing mass are calculated as follows:

$$E_{\rm miss} = 2E_{\rm beam} - \Sigma E_i, \tag{3}$$

$$\vec{p}_{\rm miss} = -\Sigma \vec{p}_i, \tag{4}$$

$$M^2_{\rm miss} = E^2_{\rm miss} - |\vec{p}_{\rm miss}|^2, \tag{5}$$

where the sums are over all reconstructed particles i in the event.

In calculating the missing energy and momentum, we identify each charged particle using the lepton and hadron identification devices. We also add the neutral showers recorded in the ECL that are not matched to any charged track. Moreover, we require that the shower shape be consistent with that of a photon and the deposited energy be greater than 30 MeV for the barrel region and 50 MeV for the endcap.

If the only undetected particle in an event is the neutrino, the missing mass should be consistent with zero. Due to the presence of a tail in the missing mass distribution originating from missing particles, an asymmetric requirement $-2.0\ {\rm GeV}^2/c^4 < M^2_{\rm miss} < 3.0\ {\rm GeV}^2/c^4$ is applied. In principle, this selects events where there is only one undetected particle in the event and that missing particle is the neutrino. Neutrinos are usually produced in conjunction with charged leptons (e or μ). Therefore, the presence of two or more leptons in an event implies that the missing energy and momentum cannot be used to accurately reconstruct the neutrino from the $\bar{B}^0 \to D^+\ell^-\bar{\nu}$ decay. For this reason, we select events with only one identified lepton with $|\vec{p}_{lab}| > 0.8\ {\rm GeV}/c$. The momentum requirement helps to reduce the signal efficiency loss due to lepton misidentification, and also reduces the backgrounds from hadrons misidentified as leptons and random combinations of leptons and D^+ mesons.

Since the initial state is charge-neutral, the charges of the reconstructed tracks should sum to zero if we detect all the particles in the event and have no additional tracks. Hence, we require that the net charge, ΔQ, in the event should be close to zero to reject events with other missing charged particles. We allow $\Delta Q = \pm 1$, as well as 0, to maintain high signal efficiency.

The neutrino reconstruction can be biased by particles that go undetected by passing down the beam pipe. To reject events with such missing particles, we require $|\cos\theta_{\vec{p}_{\rm miss}}| < 0.95$, where $\theta_{\vec{p}_{\rm miss}}$ is the polar angle of the missing momentum with respect to the positron beam direction in the laboratory frame.

D^+ candidates are reconstructed in the $D^+ \to K^-\pi^+\pi^+$ decay mode. Kaon candidates are required to be positively identified by the hadron identification devices. In addition, we require kaon candidates not to be positively identified as either a lepton or a proton. If a charged particle is not positively identified as a lepton, kaon, or proton, we treat it as a pion. The three charged tracks are then geometrically fit to a D^+ decay vertex, and we reject combinations which do not form a consistent vertex. We further require $|\vec{p}_{D^+}| < 2.5$ GeV/c in order to suppress continuum background. We select $K^-\pi^+\pi^+$ combinations where the invariant mass is within 20 MeV/c^2 of the nominal D^+ mass (Figure 1).

To reduce the feed-down background from $\bar{B} \to D^{*+}X\ell^-\bar{\nu}$ decays, we reject D^+ candidates that are consistent with being produced in the decay $D^{*+} \to D^+\pi^0$. We select π^0 candidates by requiring that the two photon invariant mass be within 16.5 MeV/c^2 of the nominal π^0 mass, where the energy of each photon is required to be greater than 20 MeV. We calculate the mass difference $M_{K^-\pi^+\pi^+\pi^0} - M_{K^-\pi^+\pi^+}$ and if it is within 2 MeV/c^2 of the nominal value for a D^{*+} decay, the D^+ candidate is rejected.

A variable $\cos\theta_{B-D\ell}$ is defined as the cosine of the angle between $\vec{p}_{\bar{B}^0}$ and $\vec{p}_{D^+\ell^-}(= \vec{p}_{D^+} + \vec{p}_{\ell^-})$. It satisfies the following kinematic relation:

$$\cos\theta_{B-D\ell} = \frac{2E_{\bar{B}^0}E_{D^+\ell^-} - m^2_{\bar{B}^0} - M^2_{D^+\ell^-}}{2|\vec{p}_{\bar{B}^0}||\vec{p}_{D^+\ell^-}|}. \tag{6}$$

The signal events are distributed mostly within the physically allowed region $|\cos\theta_{B-D\ell}| < 1$, while the background events extend to a much wider range. We require that candidates have $|\cos\theta_{B-D\ell}| < 1$.

Since the resolution of the missing momentum is better than that of the missing energy, we take $(E_{\bar{\nu}}, \vec{p}_{\bar{\nu}}) = (|\vec{p}_{\rm miss}|, \vec{p}_{\rm miss})$ as the four-momentum of the neutrino. Combining the energy-momentum four-vectors for the reconstructed D^+ meson, the signal lepton and the neutrino, and using the constraint of energy-momentum conservation, we obtain the fully reconstructed B decay variables, the beam constrained mass $M_{\rm bc}$ and the energy difference ΔE defined as

$$\Delta E = (E_{D^+} + E_{\ell^-} + E_{\bar{\nu}}) - E_{\rm beam}, \tag{7}$$

$$M_{\rm bc} = \sqrt{E^2_{\rm beam} - |\vec{p}_{D^+} + \vec{p}_{\ell^-} + \alpha\vec{p}_{\bar{\nu}}|^2}. \tag{8}$$

We select events with ΔE in the range -0.2 GeV $< \Delta E < 1$ GeV; the asymmetric requirement is to reject feed-down background from $\bar{B} \to D^{*+}X\ell^-\bar{\nu}$ decays. In the calculation of $M_{\rm bc}$ (Equation 8) we correct $p_{\bar{\nu}}$ by the factor

$$\alpha = 1 + \Delta E/E_{\bar{\nu}}, \tag{9}$$

which is equivalent to imposing $\Delta E = 0$.

3.2 Background sources

The background sources fall into five categories: combinatoric, correlated, uncorrelated, misidentified lepton and continuum.

Combinatoric background: The dominant background in this analysis is the combinatoric background in the D^+ reconstruction. The amount of combinatoric background is estimated using the events in the sideband regions 1.80 GeV/c^2 $< M_{K^-\pi^+\pi^+} <$ 1.84 GeV/c^2 and 1.90 GeV/c^2 $< M_{K^-\pi^+\pi^+} <$ 1.94 GeV/c^2, shown in Figure 1.

Correlated background: If a D^+ and a lepton have the same parent B, but do not come from the signal decay $\bar{B}^0 \to D^+\ell^-\bar{\nu}$, the event is classified as correlated background. Processes such as $\bar{B}^0 \to D^{*+}\ell^-\bar{\nu}$, $\bar{B} \to D^{**}\ell^-\bar{\nu}$ and $\bar{B} \to D^{(*)}\pi\ell^-\bar{\nu}$ (nonresonant) contribute to this source. This background is estimated by MC simulation. We use the measured form factor [10] and decay rate [11] for $\bar{B}^0 \to D^{*+}\ell^-\bar{\nu}$ which constitutes the majority (89%) of this background. For $\bar{B} \to D^{**}\ell^-\bar{\nu}$ and $\bar{B} \to D^{(*)}\pi\ell^-\bar{\nu}$, the models in refs. [12] and [13] are assumed, respectively. Our assumptions for these decay rates [14] are based on existing measurements [11].

Uncorrelated background: The uncorrelated background consists of events with a real D^+ from the decay of one B meson and a real lepton from the opposite B. We also estimate this background using a MC simulation. Due to the charge correlation with the D^+, the lepton in this background is usually from a secondary decay, and is somewhat suppressed by the lepton momentum requirement.

Misidentified lepton background: In some cases, a hadron track is misidentified as a lepton. The amount of this background is estimated from data. We treat each hadron candidate track as if it were a signal lepton and weight its contribution according to the misidentification probability measured using kinematically identified hadron tracks in data.

Continuum background: The $e^+e^- \to q\bar{q}$ continuum background is estimated using MC continuum events. We also check that this estimation is statistically consistent with the off-resonance data.

3.3 Signal yield and efficiency

Figure 2 shows the $M_{\rm bc}$ distribution after all the event selection criteria described above. In this plot the points with error bars represent the on-resonance data. The background components are also shown.

We apply a final event selection requirement $M_{\rm bc} > 5.24$ GeV/c^2 to define the signal region. The overall signal efficiency is 2.69%. Table 1 lists the number of signal events and the estimated backgrounds in the signal region.

4 Measurement of $|V_{cb}|F_D(1)$

The uncertainty on the reconstructed value of y is dominated by the error on the measurement of the neutrino four-momentum. We denote the reconstructed value as $\tilde{y}$. The resolution is improved by making the correction to the momentum measurement by the factor α given in Equation 9. Using a MC simulation, the resolution of y is found to be accurately modeled by a symmetric Gaussian with $\sigma = 0.03$.

Figure 3 shows the $\tilde{y}$ distribution for data and the estimated backgrounds. After all backgrounds are subtracted, we perform a χ^2 fit to the $\tilde{y}$ distribution to obtain $|V_{cb}|F_D(1)$ and the form factor. In the fit, the χ^2 function is expressed as [15]

$$\chi^2 = \sum_{i=1}^{N_{bin}} \frac{(N_i^{obs} - \sum_{j=1}^{N_{bin}} \epsilon_{ij} N_j)^2}{{\sigma_{N_i}^{obs}}^2 + \sum_{j=1}^{N_{bin}} \sigma_{\epsilon_{ij}}^2 N_j^2}, \tag{10}$$

where N_i^{obs} is the yield in the i-th $\tilde{y}$ bin, $\sigma_{N_i}^{obs}$ is the statistical error of N_i^{obs}, N_{bin} is the number of bins and

$$N_j = N_{B\bar{B}} \mathcal{B}(D^+ \to K^-\pi^+\pi^+) \tau_{\bar{B}^0} \int_{y_j} dy \frac{d\Gamma}{dy} \tag{11}$$

is the number of decays in the j-th bin implied by the fit parameters. Here, $N_{B\bar{B}}$ is the number of $B\bar{B}$ pairs in the sample, $\mathcal{B}(D^+ \to K^-\pi^+\pi^+)$ is the $D^+ \to K^-\pi^+\pi^+$ branching fraction [11], $\tau_{\bar{B}^0}$ is the $\bar{B}^0$ lifetime [11], and $d\Gamma/dy$ is given by Equation 1. We assume a branching fraction $\mathcal{B}(\Upsilon(4S) \to B^0\bar{B}^0) = 1/2$. The efficiency matrix (ϵ_{ij}) accounts for the reconstruction efficiency and the smearing of y due to the detector resolution. The statistical uncertainty in the efficiency matrix is represented by σ_{ij}. We use ten $\tilde{y}$ bins over the range $1.00 \leq \tilde{y} \leq 1.59$.

We use a general parametrization,

$$F_D(y) = F_D(1)\{1 - \hat{\rho}_D^2(y-1) + \hat{c}_D(y-1)^2 + O(y-1)^3\}, \qquad (12)$$

which is common to many analyses [15–17]. First we fit to a linear form factor neglecting terms of $O(y-1)^2$ and higher. We find $|V_{cb}|F_D(1) = (3.83 \pm 0.35) \times 10^{-2}$ and $\hat{\rho}_D^2 = 0.69 \pm 0.14$ with a correlation coefficient $\rho(|V_{cb}|F_D(1), \hat{\rho}_D^2) = 0.96$, where the errors are statistical only. The χ^2 is 7.6 for 8 degrees of freedom. Allowing $\hat{c}_D$ to vary in the region $\hat{c}_D > 0$, we find consistent results.

Boyd *et al.* [18] and Caprini *et al.* [19] provide different form factor parametrizations based on QCD dispersion relations to constrain the form factor. In each case a relation between $\hat{\rho}_D^2$ and $\hat{c}_D$ is obtained, leaving only one free parameter, in addition to $|V_{cb}|F_D(1)$, to be extracted from the fit. They also relate higher order terms to these free parameters. Using the form factor given by Boyd *et al.*, we find $|V_{cb}|F_D(1) = (4.14 \pm 0.47) \times 10^{-2}$, $\hat{\rho}_D^2 = 1.16 \pm 0.25$ and $\hat{c}_D = 1.06 \pm 0.28$. Using the parametrization of Caprini *et al.*, we find $|V_{cb}|F_D(1) = (4.11 \pm 0.44) \times 10^{-2}$, $\hat{\rho}_D^2 = 1.12 \pm 0.22$ and $\hat{c}_D = 1.03 \pm 0.23$. The fit results are shown in Figures 4 and 5.

We use the Caprini *et al.* form factor determined from the fit to integrate the differential decay rate, $d\Gamma/dy$, over y and obtain the decay rate $\Gamma(\bar{B}^0 \to D^+\ell^-\bar{\nu}) = (13.79 \pm 0.76)$ ns^{-1}. This decay rate leads to a branching fraction $\mathcal{B}(\bar{B}^0 \to D^+\ell^-\bar{\nu}) = (2.13 \pm 0.12)\%$, where the error is statistical only. The decay rate Γ is not sensitive to the choice of form factor parametrization. Table 2 summarizes the different fit results.

5 Systematic uncertainty

The systematic uncertainties are given in Table 3. The dominant uncertainty is the imperfection of the detector simulation for the neutrino reconstruction, which is determined by varying a number of simulation parameters including the track finding efficiency, the track momentum resolution, the fraction of incorrectly reconstructed tracks, the photon finding efficiency, the photon energy resolution, the charged kaon identification efficiency, the charm semileptonic decay fraction and the K_L^0 fraction. We take a quadratic sum of all components.

Since we rely on MC simulation to estimate the correlated backgrounds, we vary the relative fractions of $D^*\ell\nu$, $D^{**}\ell\nu$ and $D^{(*)}\pi\ell\nu$ within the constraints of the measured exclusive and inclusive semileptonic branching fractions [11]. To determine the uncertainty from the $\bar{B}^0 \to D^{*+}\ell^-\bar{\nu}$ form factor, we vary

the form factor within the uncertainties of the measurement [10] while taking into account the correlations among the parameters.

The uncorrelated, continuum and misidentified lepton backgrounds are very small, hence even assuming large uncertainties in these backgrounds makes a negligible difference in our result.

The remaining contributions to the systematic uncertainty are the uncertainty in the D^+ vertexing efficiency, and the uncertainties in the lepton finding efficiency, number of $B\bar{B}$ pairs, $D^+ \to K^-\pi^+\pi^+$ branching fraction and the $\bar{B}^0$ lifetime.

We have tested the stability of the result by varying several of the selection criteria; in each case no significant change is observed. Furthermore, the results obtained with the e^- channel and with the μ^- channel are consistent.

6 Summary

Using the missing energy and momentum to extract kinematic information about the undetected neutrino in the $\bar{B}^0 \to D^+\ell^-\bar{\nu}$ decay, we have measured the decay rate, $|V_{cb}|F_D(1)$ and the form factor parameters for a number of different parametrizations. These results, with statistical errors, are summarized in Table 2. We have evaluated systematic errors of 12.5%, 12.6% and 18.2% on $|V_{cb}|F_D(1)$, $\hat{\rho}^2_D$ and Γ respectively. Using the Caprini *et al.* parametrization, we find the decay rate of $\bar{B}^0 \to D^+\ell^-\bar{\nu}$,

$$\Gamma(\bar{B}^0 \to D^+\ell^-\bar{\nu}) = (13.79 \pm 0.76 \pm 2.51)\ \mathrm{ns}^{-1},$$

corresponding to the branching fraction,

$$\mathcal{B}(\bar{B}^0 \to D^+\ell^-\bar{\nu}) = (2.13 \pm 0.12 \pm 0.39)\%,$$

and we find the rate normalization,

$$|V_{cb}|F_D(1) = (4.11 \pm 0.44 \pm 0.52) \times 10^{-2}.$$

Using $F_D(1) = 0.98 \pm 0.07$ [19], we find

$$|V_{cb}| = (4.19 \pm 0.45 \pm 0.53 \pm 0.30) \times 10^{-2}.$$

where the last error comes from the theoretical uncertainty of $F_D(1)$. These results are consistent with the result of $\bar{B}^0 \to D^{*+}e^-\bar{\nu}$ analysis from Belle [20]

and with the existing measurements [15–17,21–23]

From the results of $\bar{B}^0 \to D^{*+} e^- \bar{\nu}$ analysis at Belle, the ratio of $F_D(1)$ and $F_{D^*}(1)$ and the difference between $\hat{\rho}^2_D$ and $\hat{\rho}^2_{D^*}$ are measured to be

$$\frac{F_D(1)}{F_{D^*}(1)} = \begin{cases} 1.12 \pm 0.12 \pm 0.12 \text{ (Linear form factor)} \\ 1.16 \pm 0.14 \pm 0.12 \text{ (Caprini } \textit{et al.} \text{ form factor)}, \end{cases}$$

$$\hat{\rho}^2_D - \hat{\rho}^2_{D^*} = \begin{cases} -0.12 \pm 0.18 \pm 0.13 \text{ (Linear form factor)} \\ -0.23 \pm 0.29 \pm 0.20 \text{ (Caprini } \textit{et al.} \text{ form factor)}, \end{cases}$$

where the first error is statistical and the second is systematic after removing the correlated error terms between the two analyses. These results are in agreement with theoretical predictions [19,24,25].

7 Acknowledgements

We thank Benjamin Grinstein for useful discussions. We wish to thank the KEKB accelerator group for the excellent operation of the KEKB accelerator. We acknowledge support from the Ministry of Education, Culture, Sports, Science, and Technology of Japan and the Japan Society for the Promotion of Science; the Australian Research Council and the Australian Department of Industry, Science and Resources; the Department of Science and Technology of India; the BK21 program of the Ministry of Education of Korea and the Center for High Energy Physics sponsored by the KOSEF; the Polish State Committee for Scientific Research under contract No.2P03B 17017; the Ministry of Science and Technology of Russian Federation; the National Science Council and the Ministry of Education of Taiwan; and the U.S. Department of Energy.

References

[1] N. Cabibbo, Phys. Rev. Lett. **10**, 531 (1963); M. Kobayashi and T. Maskawa, Prog. Theor. Phys. **49**, 652 (1973).

[2] N. Isgur and M. B. Wise, Phys. Lett. **B232**, 113 (1989); M. Neubert, Phys. Rep. **245**, 259 (1994).

[3] M. Neubert, Phys. Lett. **B264**, 455 (1991).

[4] Z. Ligeti, Y. Nir, and M. Neubert, Phys. Rev. **D49**, 1302 (1994).

[5] K. Abe *et al.* (Belle Collaboration), KEK Progress Report 2000-4 (2000), to be published in Nucl. Inst. and Meth. A.

[6] KEKB B Factory Design Report, KEK Report 95-7 (1995), unpublished; Y. Funakoshi *et al.*, Proc. 2000 European Particle Accelerator Conference, Vienna (2000).

[7] We use GEANT3 for the detector simulation: CERN Program Library Long Writeup W5013, CERN, 1993.

[8] G. Fox and S. Wolfram, Phys. Rev. Lett. **41**, 1581 (1978).

[9] J. P. Alexander *et al.* (CLEO Collaboration), Phys. Rev. Lett. **77**, 5000 (1996).

[10] J. E. Duboscq *et al.* (CLEO Collaboration), Phys. Rev. Lett. **76**, 3898 (1996).

[11] D. E. Groom *et al.* (Particle Data Group), Eur. Phys. J. **C15**, 1 (2000).

[12] N. Isgur and D. Scora, Phys. Rev. **D52**, 2783 (1995); N. Isgur, D. Scora, B. Grinstein, and M. B. Wise, Phys. Rev. **D39**, 799 (1989).

[13] J. L. Goity and W. Roberts, Phys. Rev. **D51**, 3459 (1995).

[14] We assume decay rates $\mathcal{B}(\bar{B} \to D_0^* \ell\bar{\nu}) = 0.04\%$, $\mathcal{B}(\bar{B} \to D_1^* \ell\bar{\nu}) = 0.04\%$, $\mathcal{B}(\bar{B} \to D_1 \ell\bar{\nu}) = 0.26\%$, $\mathcal{B}(\bar{B} \to D_2^* \ell\bar{\nu}) = 0.13\%$, $\mathcal{B}(\bar{B} \to D' \ell\bar{\nu}) = 0.01\%$, $\mathcal{B}(\bar{B} \to D^{*\prime} \ell\bar{\nu}) = 0.09\%$, $\mathcal{B}(\bar{B}^0 \to D^+ \pi^0 \ell^- \bar{\nu}) = 0.32\%$, $\mathcal{B}(B^- \to D^+ \pi^- \ell^- \bar{\nu}) = 0.64\%$, $\mathcal{B}(\bar{B} \to D^{*+} \pi^0 \ell^- \bar{\nu}) = 0.45\%$, $\mathcal{B}(B^- \to D^{*+} \pi^- \ell^- \bar{\nu}) = 0.89\%$.

[15] J. Bartelt *et al.* (CLEO Collaboration), Phys. Rev. Lett. **82** 3746 (1999).

[16] M. Athanas *et al.* (CLEO Collaboration), Phys. Rev. Lett. **79**, 2208 (1997).

[17] D. Buskulic *et al.* (ALEPH Collaboration), Phys. Lett. **B395**, 373 (1997).

[18] C. G. Boyd, B. Grinstein and R. F. Lebed, Phys. Rev. **D56**, 6895, (1997).

[19] I. Caprini, L. Lellouch and M. Neubert, Nucl. Phys. **B530** 153, (1998).

[20] K. Abe *et al.* (Belle Collaboration), hep-ex/0111060, submitted to Phys. Lett. **B**.

[21] G. Abbiendi *et al.* (OPAL Collaboration), Phys. Lett. **B842**, 15, (2000).

[22] P. Abreu *et al.* (DELPHI Collaboration), Phys. Lett. **B510**, 55, (2001).

[23] J. P. Alexander *et al.* (CLEO Collaboration), hep-ex/0007052, CLEO-CONF-00-03 (2000).

[24] Z. Ligeti, Y. Nir and M. Neubert, Phys. Rev. **D49**, 1302 (1994).

[25] S. Hashimoto *et al.*, Phys. Rev. **D61**, 14502 (1999); S. Hashimoto *et al.*, hep-ph/0110253, FERMILAB-PUB-01/317-T.

Table 1
Numbers of signal and background events in the signal region after all event selection requirements.

Total yield	2518 ± 50
Combinatoric background	983 ± 22
Correlated background	349 ± 14
Uncorrelated background	35 ± 4
Misidentified lepton background	9 ± 1
Continuum background	43 ± 7
Final signal yield	1099 ± 57

Table 2
Summary of the results of the $d\Gamma/dy$ fit.

Model	$\lvert V_{cb}\rvert F_D(1)/10^{-2}$	$\hat{\rho}_D^2$	$\hat{c}_D$	$\Gamma(\mathrm{ns}^{-1})$	χ^2/dof
Linear	3.83 ± 0.35	0.69 ± 0.14	0	13.76 ± 0.76	7.6/8
Curvature	$3.83\ ^{+\ 0.46}_{-\ 0.35}$	$0.69\ ^{+\ 0.42}_{-\ 0.15}$	$0.00\ ^{+\ 0.59}_{-\ 0.00}$	13.76 ± 0.76	7.6/7
Boyd *et al.*	4.14 ± 0.47	1.16 ± 0.25	1.06 ± 0.28	13.78 ± 0.76	8.4/8
Caprini *et al.*	4.11 ± 0.44	1.12 ± 0.22	1.03 ± 0.23	13.79 ± 0.76	8.2/8

Table 3
Summary of the relative systematic errors.

Source of uncertainty	$\Delta\lvert V_{cb}\rvert F_D(1)$ (%)	$\Delta\hat{\rho}_D^2$ (%)	$\Delta\Gamma$ (%)
ν reconstruction simulation	10.6	9.7	15.5
Correlated background normalization	2.4	4.4	1.9
D^* form factor	1.5	2.8	0.9
Other background normalization	0.6	1.8	0.4
D^+ vertexing efficiency	4.7	5.8	5.3
Lepton finding efficiency	1.5	-	3.0
$N_{B\bar{B}}$	0.5	-	1.0
$Br(D^+ \to K^-\pi^+\pi^+)$	3.3	-	6.7
$\tau_{\bar{B}^0}$	1.0	-	2.1
Total	12.5	12.6	18.2

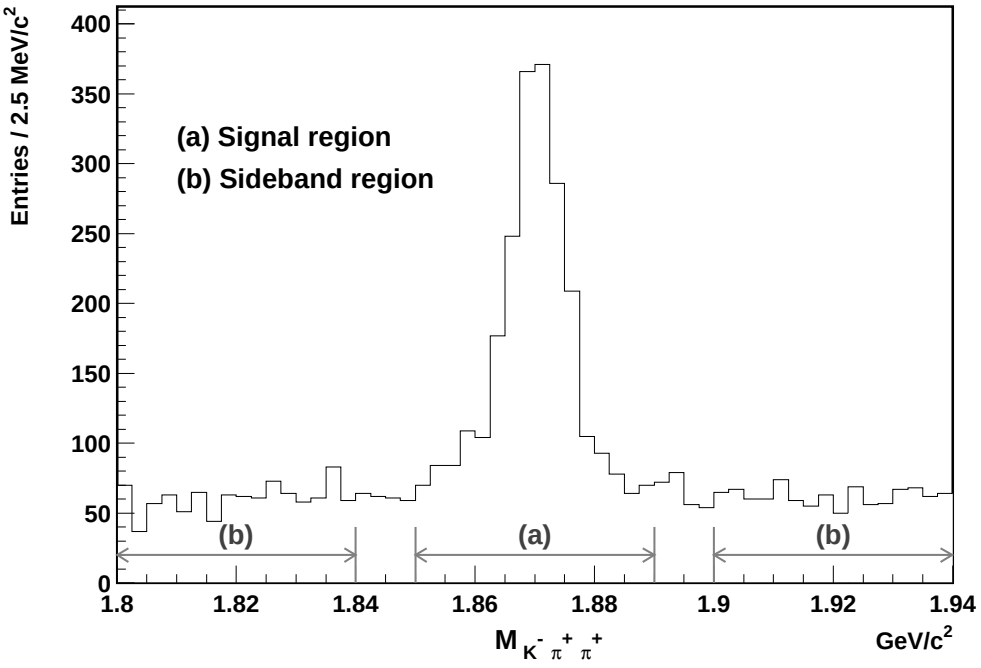

Fig. 1. $M_{K^-\pi^+\pi^+}$ distribution after all event selection criteria except the $M_{K^-\pi^+\pi^+}$ requirement. The signal region is indicated by (a) and the sideband regions by (b).

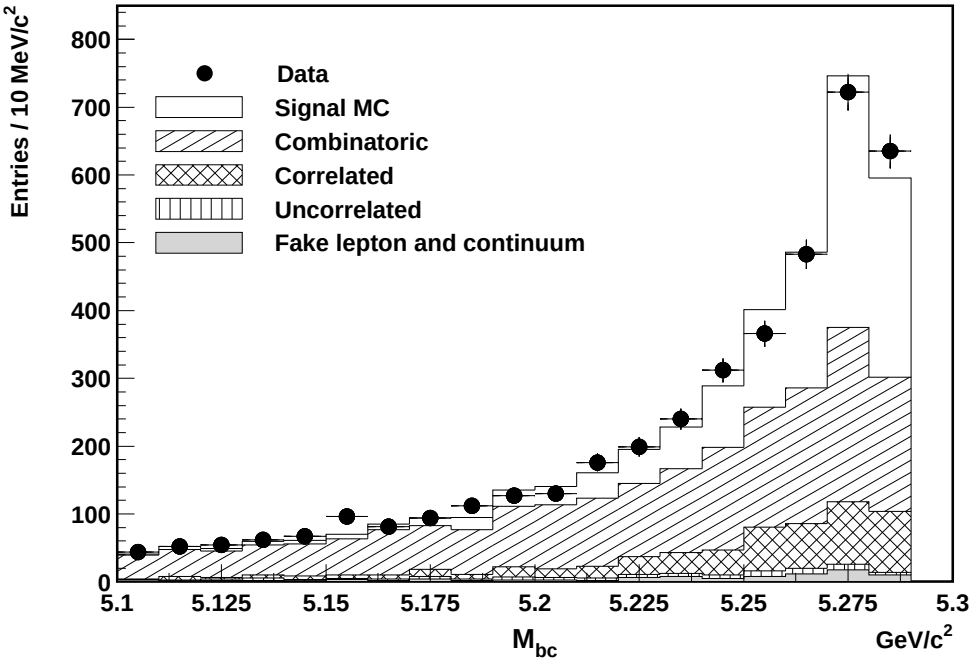

Fig. 2. $M_{\rm bc}$ distribution and estimated backgrounds. The points with error bars show the data. The shaded component is the continuum and fake lepton background, the vertically hatched histogram is the uncorrelated background, the cross-hatched histogram is the correlated background, and the diagonal hatched histogram is the combinatoric background. The open histogram is the signal MC, normalized to the measured decay rate.

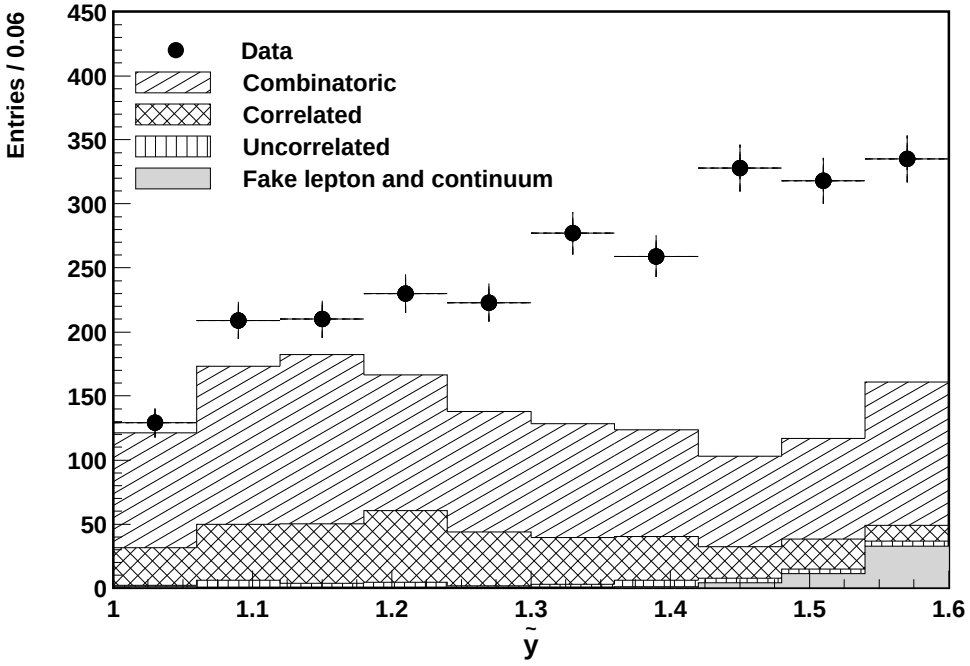

Fig. 3. $\tilde{y}$ distribution after the $M_{\rm bc} > 5.24$ GeV/c^2 requirement. The histogram shadings are the same as those in Figure 2.

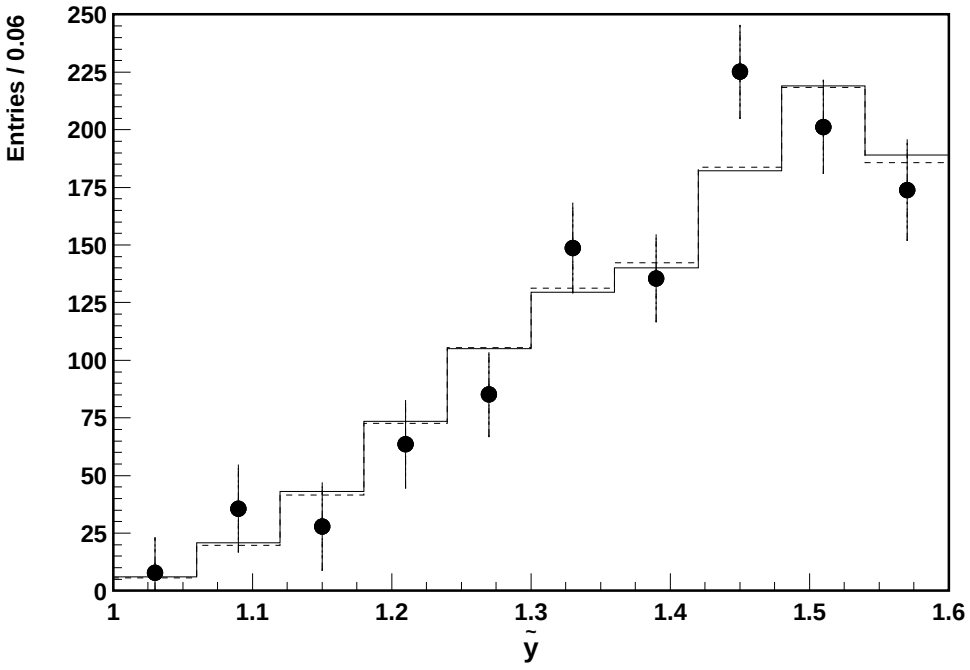

Fig. 4. $\tilde{y}$ distribution and fit. The points with error bars are data after background subtraction. The dashed histogram is the fit result for the linear form factor. The solid histogram is the fit result for the dispersion relation (Caprini *et al.*) form factor.

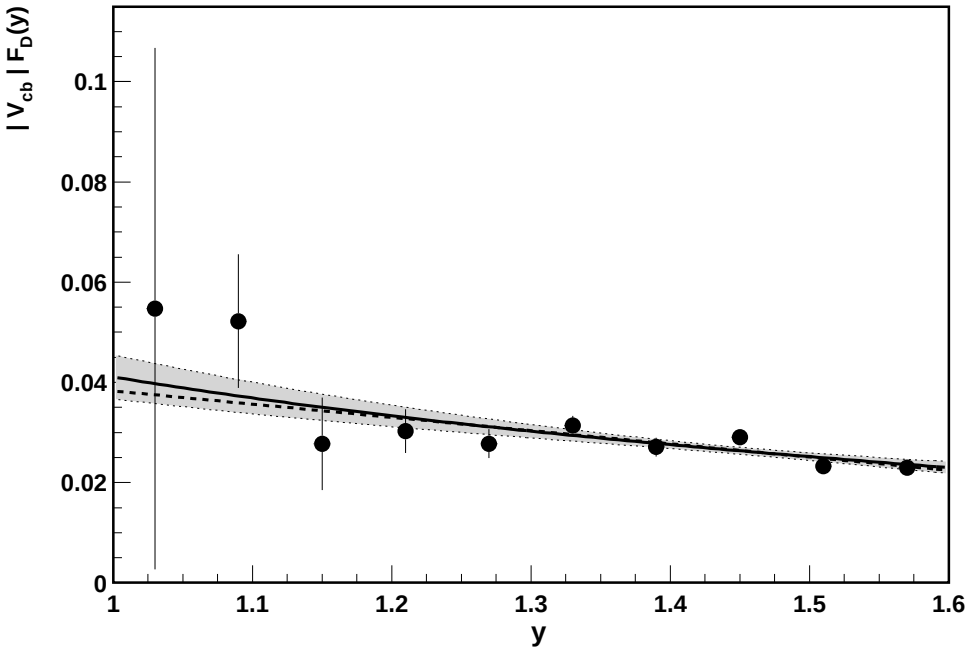

Fig. 5. $|V_{cb}|F_D(y)$ as a function of y. The points with error bars are the data; the curves are fit results for the linear form factor (dashed) and the Caprini *et al*. form factor (solid). The shaded band indicates the statistical uncertainty for the Caprini *et al*. form factor fit.